Role of magnetic/nonmagnetic semiconductor interfaces in magneto-optical properties of small-offset superlattices

M. Syed, G. L. Yang, J. K. Furdyna, and M. Dobrowolska
Department of Physics, University of Notre Dame, Notre Dame, Indiana 46556

S. Lee
Department of Physics, Korea University, Seoul, 136-701, Korea

L. R. Ram-Mohan
Departments of Physics and Electrical and Computer Engineering, Worcester Polytechnic Institute, Worcester, Massachusetts 01609
(Received 26 April 2002; published 30 August 2002)

$Zn_{1-x}Mn_xSe/ZnSe$ superlattices (SL's) involving magnetic/nonmagnetic interfaces were investigated by magnetoabsorption spectroscopy. The Mn concentration in the $Zn_{1-x}Mn_xSe$ layers ranged from $x=0.10$ to 0.14, resulting in small band offsets between barriers and wells of the SL's. The data were analyzed using the eight-band $\mathbf{k}\cdot\mathbf{p}$ model and the finite element method, taking into account interdiffusion of elements across the interface. We found that the Zeeman shifts of the ground- and excited-state transitions observed in all superlattices can be successfully explained by a single common profile of the graded interface, that extends over about three monolayers. In addition, the data revealed the presence of antiferromagnetic coupling between Mn ions across thin (less than 18 Å) ZnSe layers in the above $Zn_{1-x}Mn_xSe/ZnSe$ multilayer structures.

DOI: 10.1103/PhysRevB.66.075213 PACS number(s): 71.20.Nr, 78.66.Hf, 75.50.Pp

I. INTRODUCTION

The study of semiconductor heterostructures constitutes a continually expanding area of research, that has resulted in a large number of developments both in fundamental physics and in technology. Heterostructures necessarily involve interfaces, and recently a number of papers[1–8] pointed to the fact that to understand semiconductor multilayer structures, one must go beyond the idealized picture that such interfaces are simply steplike. Structural studies, such as x-ray diffraction,[9] electron microscopy,[10] or scanning tunneling microscopy,[11] support this conclusion. Specifically, these methods indicate that there occurs significant interdiffusion across the interface, resulting in graded rather than steplike composition profiles at the interface. Such a graded transition from one material to the other will in turn alter the potential profile, thus affecting the electronic and optical properties of semiconductor heterostructures. It is therefore important to have the ability to estimate how elements are distributed when an interface is formed.

Recently a method was developed[4] that allows one to map the profile of an interface when it consists of a diluted magnetic semiconductor (DMS) and a nonmagnetic semiconductor. DMSs are semiconducting alloys in which a part of the crystal lattice is comprised of substitutionall magnetic ions.[12] The best known examples of such materials are $II_{1-x}Mn_xVI$ alloys (e.g., $Zn_{1-x}Mn_xSe$ and $Cd_{1-x}Mn_xTe$). One of the remarkable properties of these systems is that they exhibit extremely large Zeeman splittings of the band edges due to spin-spin exchange interaction between the *d* electrons of the Mn^{2+} ions and the *s*- or *p*-band electrons. Quantum wells and superlattices made up of DMS and non-DMS layers thus provide an excellent laboratory for studying interfaces, because the Zeeman splitting of a given electronic state in such a system will depend on the number of magnetic ions ''seen'' by the wave function of that state. For example, if the interface is steplike the Zeeman splitting of an exciton in a deep nonmagnetic quantum well between DMS barriers should be small because of the small penetration of the exciton wave function into the barriers. But if diffusion of Mn occurs across the interface into the well layer, the exciton wave function overlaps significantly with a larger number of magnetic ions, thus leading to a considerable enhancement of the Zeeman splitting. Gaj *et al.*[4] studied the ground-state exciton in relatively deep CdTe wells between $Cd_{1-x}Mn_xTe$ barriers, and observed a pronounced Zeeman splitting enhancement, that they attributed to the diffusion of magnetic ions into the well region. Quantitative analysis of this effect made it possible to map out the $CdTe/Cd_{1-x}Mn_xTe$ interface profile with impressive detail. One should note that, with the discovery of ferromagnetism in semiconductors containing Mn the understanding of the DMS/non-DMS interface has acquired added importance since the operation of spin-based devices, such as spin valves or spin injectors, will be highly sensitive to the interface properties.

In this paper we describe the results of magnetoabsorption experiments on shallow-well $ZnSe/Zn_{1-x}Mn_xSe$ superlattices, where *a very large fraction* of the wave function penetrates into the DMS barriers. This geometry is thus particularly sensitive to interactions of the electronic states with magnetic ions in the vicinity of the interface. In these experiments we were, furthermore, able to observe transitions involving *excited states*, whose wave functions penetrate into the interface region to an even higher degree than the ground states. The magnetic-field dependence of the transition energies involving those excited states will therefore be especially sensitive to the shape of the band profile (especially for narrow wells), allowing a more detailed mapping of the interface region.

TABLE I. Sample description.

Sample	ZnSe layer thickness (Å)	$Zn_{1-x}Mn_xSe$ layer thickness (Å)	x	Number of periods
1	60	20	0.10	20
2	25	25	0.10	20
3	80	40	0.10	20
4	40	60	0.10	20
5	40	80	0.10	20
6	40	20	0.145	30
7	30	30	0.145	30
8	80	40	0.145	30
9	50	50	0.145	30
10	40	60	0.145	30
11	40	80	0.145	30

II. EXPERIMENT

Two series of ($ZnSe/Zn_{1-x}Mn_xSe$ superlattices were grown by molecular-beam epitaxy MBE) on GaAs(001) substrates, after first depositing a 1-μm ZnSe buffer layer. Structural parameters describing the superlattices are listed in Table I. The first series (samples 1–5) consists of five 20-period superlattices with a Mn concentration of 10% ($x=0.10$) in the $Zn_{1-x}Mn_xSe$ layers. In the second series (samples 6–11) the Mn concentration is slightly higher (14.5%), and the number of periods is 30. The superlattices were designed with an eye toward understanding of the role of interfaces, by varying the thickness ratio of the two constituent materials from wide wells with narrow barriers to narrow wells with wide barriers. The thicknesses of the layers listed in the table are estimated from the growth time, assuming the same growth rates for all samples. In order to determine the Mn concentration in the $Zn_{1-x}Mn_xSe$ layers, ''companion'' $Zn_{1-x}Mn_xSe$ epilayers were grown for each sample series under the same MBE growth conditions as those used for the superlattices.

For transmission experiments, the GaAs substrate was removed from the samples by mechanical polishing, followed by chemical etching. As the etchant we used a solution of NH_4OH in H_2O_2 in a 1:10 ratio at 30 °C. In addition to removing the remaining substrate material, the etching process also removed the dislocation-rich region of the ZnSe buffer near the ZnSe/GaAs interface. The magnetoabsorption experiments were performed in an optical cryostat ($T \geqslant 1.5$ K) equipped with a 6-T superconducting magnet. The light source consisted of a halogen lamp and a 1-m monochromator. The monochromatic light was circularly polarized, so as to distinguish transitions involving different spin states. The transmitted light signal was detected by a photomultiplier tube, amplified by a lock-in amplifier, and sent to data-acquisition software for processing and analysis.

III. OVERVIEW OF EXPERIMENTAL RESULTS

Figure 1 shows magnetoabsorption spectra for sample 5 (see Table I) observed for several magnetic fields in the σ^+ circular polarization, taken by sweeping the wavelength of the incident light and recording the transmitted intensity at fixed values of the field. The strong absorption peak observed at the lowest energy (labeled *a*) corresponds to the $1s$ ground-state exciton transition, involving the first spin-down heavy-hole superlattice state (spin-down hh1; $J_z=-\frac{3}{2}$) and the first electron state (spin-down $e1$; $J_z=-\frac{1}{2}$), both at the center of the Brillouin zone ($q=0$). The peak immediately adjacent to it (labeled *b*) corresponds to the $2s$ transition of the same ground-state exciton. Peaks labeled *c* are identified as transitions involving higher superlattice states. Transitions occurring at higher energies (near 2.80 eV and above) arise from the ZnSe buffer layer.

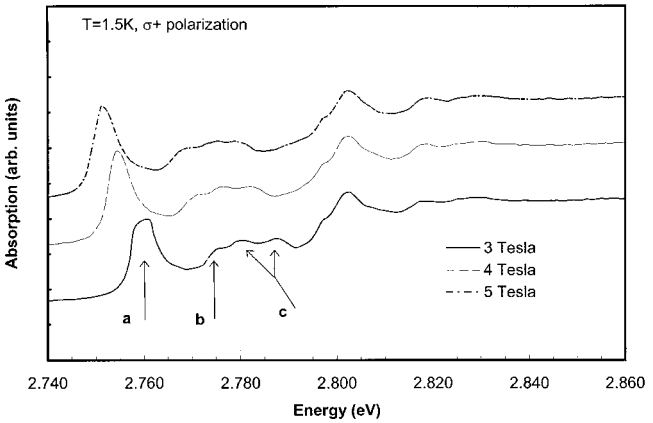

FIG. 1. Absorption spectra for sample 5 observed at 1.5 K for the σ^+ circular polarization at several magnetic fields.

The above identifications are made on the basis of the behavior of the absorption peak in an external magnetic field. Transitions originating from the superlattice depend on the magnetic field due to the large Zeeman shifts in the $Zn_{1-x}Mn_xSe$ layers, as will be discussed in Sec. IV, and transitions originating from the ZnSe buffer are field independent. This provides a convenient way of distinguishing between transitions occurring in different spatial regions of the structure.

Figure 2 shows magnetoabsorption spectra for sample 5 observed for several magnetic fields in the σ^- circular po-

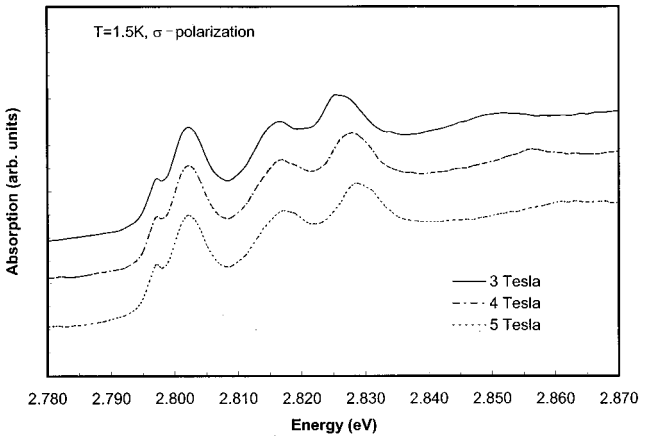

FIG. 2. Absorption spectra for sample 5 observed at 1.5 K for the σ^- circular polarization at several magnetic fields.

larization. The peak (in the vicinity of 2.85 eV at 3 T), exhibiting a strong magnetic-field dependence, corresponds to the transition between spin-up hh1 and $e1$ states at the edge of Brillouin zone of the superlattice. The strong (magnetic-field-independent) absorption peaks observed at lower energies originate from the ZnSe buffer layer. The spectra exhibited by the remaining samples used in this study are qualitatively identical to those shown in Figs. 1 and 2.

IV. METHOD OF CALCULATION

The optical transition energy from the nth heavy hole state to the mth state in the conduction band of a superlattice is expressed as

$$E_{nm}=E_g^{\text{well}}+E_n+E_m-E_{nm}^B, \tag{1}$$

where E_g^{well} is the band gap of the well material, E_n and E_m are the confinement energies of the heavy hole and the electron states, respectively, and E_{nm}^B is the binding energy of the exciton. E_n and E_m were calculated using the transfer-matrix algorithm based on an eight-band $\mathbf{k}\cdot\mathbf{p}$ model,[13] with the inclusion of the deformation-potential term.[14] In order to calculate the transition energies in an external magnetic field, the $\mathbf{k}\cdot\mathbf{p}$ program was modified to include the exchange Hamiltonian, which accounts for the interactions between the band electrons and the localized Mn spins in the $Zn_{1-x}Mn_xSe$ layers.[1,15,16] The resulting Schrödinger equation is a complicated 8×8 matrix, and cannot be solved analytically. To solve the problem, we use the so called "finite element method" [17]—a numerical technique which has proven immensely useful in dealing with the electronic structure of superlattices. This method has the advantage that a great number of perturbations and experimental conditions (such as strain, compositional profile, and magnetic fields) can be included with relative ease into the analysis. Each physical region of the structure under consideration is represented by a finite element, and the accuracy of modeling as a whole can be increased by increasing the number of elements representing that physical region. In our calculations we exploit this property extensively for modeling the profile of the Mn concentration at the interface by using a sequence of elements with different Mn concentrations, as will be discussed later.

In our case, the model involves the following parameters (all listed in Table II): the band parameters; the energy gap E_g, the energy of the s-p interaction, E_p; the spin-orbit splitting Δ, parameters γ_1, γ_2, γ_3, and κ, which describe interactions between the Γ_8 band and distant bands for both ZnSe and $Zn_xMn_{1-x}Se$; and strain parameters a_c, a_v, b_v, C_{11}, and C_{12}. For the conduction- and valence-band offsets (V_c and V_v), we have assumed (following Klar *et al.*[18]) that 20% of the band-gap difference between unstrained ZnSe and $Zn_xMn_{1-x}Se$ is accommodated by the valence band. The well and barrier thicknesses are also included in the model, and are treated in our calculations as adjustable parameters in the fitting process.

Our model also involves four magnetic parameters describing the exchange interaction in DMS layers: $N_o\alpha$, $N_o\beta$, x_{eff}, and T_0.[12] Here $N_o\alpha$ and $N_o\beta$ are the exchange integrals for the conduction and valence bands, respectively. The parameters x_{eff} and T_0, introduced in Ref. 19 are useful in describing the Zeeman shift of the DMS band edges in the Mn concentration range where the antiferromagnetic interactions between neighboring Mn^{2+} ions becomes significant. In this model the Mn mole fraction x is replaced by an effective Mn concentration x_{eff}, and the temperature T in the Brillouin function is replaced by an effective temperature T_0.[12] Both parameters (x_{eff} and T_0) for the companion epilayers were determined from the observed Zeeman splitting and are listed in Table II. Parameters x_{eff} and T_0 provide an empirical measure of antiferromagnetic interactions between the Mn^{2+} spins in the DMS material. The relationship between x_{eff} and x over the range $0<x<0.8$ has been investigated by Fatah *et al.*,[20] who performed numerical simulations of the antiferromagnetic spin pairing between neighboring magnetic ions. In Fig. 3 we show a plot of the effective Mn concentration x_{eff} as a function of x obtained via a simulation that includes only nearest-neighbor pairing, and we compare this to experimental data for $Zn_{1-x}Mn_xSe$ epilayers obtained by us, showing that the agreement between the calculated and experimental values of x_{eff} is excellent.

Here one should note that at the DMS/non-DMS interface the number of antiferromagnetic neighbors surrounding a Mn^{2+} ion is reduced. This reduction translates into a corresponding reduction of antiferromagnetic pair population, leading to an *enhancement* of Zeeman splitting of the electronic states. The dashed line in Fig. 3 shows of x_{eff} calcu-

TABLE II. Materials parameters used in the calculations. Values of $N_o\alpha$ and $N_o\beta$ are taken from Ref. 15, and x_{eff} and T_O are determined from the observed Zeeman splitting.

Parameters	ZnSe	$Zn_{0.90}Mn_{0.10}Se$	$Zn_{0.86}Mn_{0.14}Se$
Band parameters (from Ref. 24)			
E_g (eV)	2.802	2.808	2.818
E_p (eV)	29.7	29.7	29.7
Δ (eV)	0.403	0.403	0.403
γ_1	4.3	4.3	4.3
γ_2	1.14	1.14	1.14
γ_3	1.84	1.84	1.84
κ	0.2	0.2	0.2
Strain parameters (from Ref. 25)			
a_c (eV)	−3.35	−3.35	−3.35
a_v (eV)	−1.25	−1.25	−1.25
b_v (eV)	−1.17	−1.17	−1.17
C_{11} (dyn/cm^2)	8.88×10^{11}	8.88×10^{11}	8.88×10^{11}
C_{12} (dyn/cm^2)	5.27×10^{11}	5.27×10^{11}	5.27×10^{11}
Magnetic parameters			
$N_o\alpha$ (eV)	—	−0.293	−0.293
$N_o\beta$ (eV)	—	0.88	0.88
T_o (K)	—	2.15	2.15
x_{eff} (%)	—	4.2	4.2

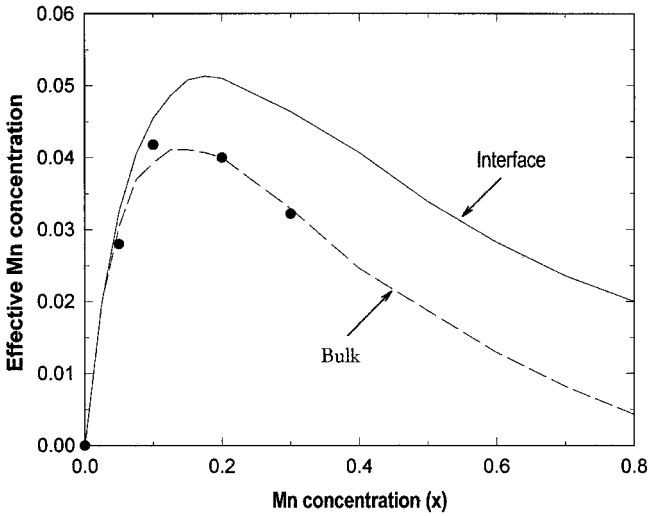

FIG. 3. The relation between x and x_{eff} in bulk DMS's and at a DMS/non-DMS interface, shown as solid and dotted curves, respectively (after Ref. 16). The enhancement of paramagnetism at the interface is clear for a Mn concentrations x above 0.10. The solid dots correspond to experimental values obtained by the authors on a series of $Zn_{1-x}Mn_xSe$ epilayers.

lated for $Zn_{1-x}Mn_xSe$/ZnSe interface by Fatah *et al.*[20] The figure clearly shows that x_{eff} is higher for an interface than for the bulk for $x \approx 0.10$ and higher.

The term E^B_{nm} in Eq. (1) is the exciton binding energy. Our superlattices are characterized by small offsets, such that the depths of the quantum wells are smaller or comparable to E^B_{nm}. Such systems are difficult to analyze, because the methods developed for calculating exciton binding energies in deep quantum wells no longer apply, and variational methods are tedious and subject to various approximations.[21] Moreover, the exciton binding energies in our samples are expected to vary with magnetic field due to field-induced changes in the barrier height. In order to evaluate exciton binding energies and their magnetic-field dependence, we have therefore resorted to an alternative approach—the so-called 'fractional dimensional analysis' [22]—that appears particularly well suited to the present situation. The appeal of this method lies in the possibility of using the experimentally observed energy difference ΔE between the $1s$ and $2s$ states of an exciton observed on the sample in question, to establish the exciton binding energy for that sample at any given value of magnetic field, without the necessity of knowing the precise details of the potential profile of the superlattice, and its magnetic field dependence. The details of that approach are given elsewhere.[23]

V. RESULTS: QUANTITATIVE ANALYSIS

In order to interpret our data we first calculated the ground-state energy of the exciton for all samples at zero magnetic field. For the energy gap values of $Zn_{1-x}Mn_xSe$ layers in the two superlattice series we used the values determined from the spectra measured on the companion epilayers: 2.808 eV for $x=0.10$ and 2.818 eV for $x=0.145$. The biaxial strain within the individual layers was calculated using the following strategy. Since the total thicknesses of all superlattices used in the present study exceed the critical thickness for the corresponding ZnSe/$Zn_{1-x}Mn_xSe$ combinations, we treated the structures as free-standing superlattices, with a common in-plane lattice constants a_p given by the equation

$$a_p=(a_1d_1+a_2d_2)/(d_1+d_2), \tag{2}$$

where a_1 and a_2 are the lattice constants of bulk ZnSe and $Zn_{1-x}Mn_xSe$, respectively, and d_1 and d_2 are their respective layer thicknesses in a given superlattice. This common in-plane lattice constant a_p is now used to determine the biaxial strain in a given layer

$$\varepsilon_{xx}=\varepsilon_{yy}=(a_p-a_i)/a_p, \tag{3}$$

i.e., the strain in the ZnSe layer is obtained with $a_i=a_1$, and in the $Zn_{1-x}Mn_xSe$ layer with $a_i=a_2$. The resulting strain is compressive for $Zn_{1-x}Mn_xSe$ layers and tensile for ZnSe layers. Since the value of a_p depends on relative layer thicknesses, which vary from sample to sample, the strain conditions will also show slight variations for different samples within a series with the same Mn concentration.

The band and strain parameters for the constituent layers of the superlattices were taken from the literature, and are listed in Table II. Taking these as fixed, we fit the calculated ground state exciton energies to the observed values in the absence of magnetic field, using the well and barrier thickness as *the only* adjustable parameters in the fitting process. It was sufficient to vary these thicknesses by not more than 5% of their nominal values listed in Table I to obtain good agreement between the measured and the calculated transition energies. For the calculations in the absence of magnetic field we assumed an abrupt interface, in order to minimize the number of fitting parameters at this stage. Since the band-gap difference between constituent materials is very small (see Table II), the energy of the ground state transition is fairly insensitive to the shape of an interface profile justifying this assumption.

In Fig. 4 (center diagram) we show the schematic band alignment at zero magnetic field for the superlattices studied. There are, of course, slight quantitative variations in the initial configuration from sample to sample due to slightly different strain conditions. However, all superlattices have a staggered type-II configuration at $B=0$ in both superlattice series, the valence-band wells being in the DMS layers and the conduction-band wells in the ZnSe layers. In both series the valence-band offsets are shallow (6–7 meV), while in the conduction band the offsets are deeper (about 17 meV in the first series and about 37 meV in the second).

The above band alignment changes significantly in the presence of a magnetic field due to the very large Zeeman splitting of the band edges in the $Zn_{1-x}Mn_xSe$ layers, as shown in the left- and right-hand diagrams in Fig. 4. For states with a spin-down orientation (which correspond to observations in the σ^+ circular polarization), the valence-band conduction-band edges move toward each other in the $Zn_{1-x}Mn_xSe$ layers, resulting in an increase in the valence-

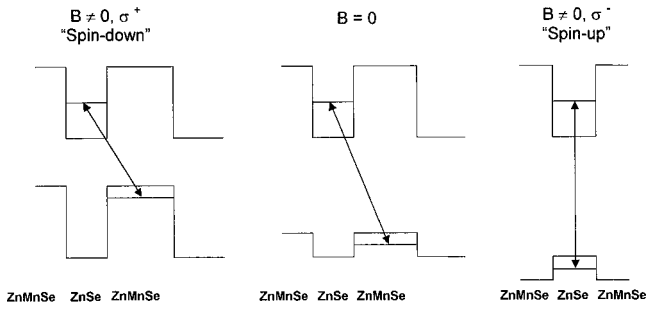

FIG. 4. Band alignment for the superlattices used in this study. The center diagram shows the initial type-II (staggered) configuration at $B=0$, with holes confined in DMS layers and electrons in ZnSe layers. When a magnetic field is applied, large Zeeman splitting of the band edges occurs in the DMS layer. As a result, the alignment remains of type-II for ''spin-down'' states (diagram on the left), while for ''spin-up'' states (right) the band alignment transforms to type-I, such that holes and electrons are now both confined in the ZnSe layers. The allowed ground-state optical transitions corresponding to these configurations are shown by arrows.

band offsets (up to 50 meV at $B=5$ T), and a decrease of the offset in the conduction band. However, the system still retains its type-II character for the spin-down orientation. This results in very tightly confined holes in the DMS layers, and rather weakly localized electrons in the ZnSe layers. For the spin-up orientation, however, the small initial valence-band offset of about 6 meV is very quickly overturned even at low magnetic fields (at about 0.25 T). Above this field the ZnSe layers become the confining layers for the holes as well as for the electrons; and the conduction electron wells (which were already in the ZnSe layers) grow deeper. Thus the system as a whole now exhibits a *type-I band alignment*, the ZnSe layers acting as wells in both bands for the spin-up carriers.

While computing transition energies in the presence of an applied magnetic field, we assumed a graded interface to account for diffusion of Mn ions across DMS/non-DMS interfaces. As was shown for a variety of DMS/non-DMS heterostructures,[1–5,15,26–29] Mn interdiffusion results in a marked enhancement of Zeeman splitting in those systems. In the analysis, therefore, we carried out eight-band $\mathbf{k}\cdot\mathbf{p}$ calculations in the presence of an magnetic field with the same parameters and layer thickness that gave us the best fit to the zero-field spectra, but using several different error-function profiles to represent the interface region. In modeling the system, we imposed the requirement that the diffusion profile should be the same in all samples, since they were all grown under identical conditions; i.e., our goal was to find a common concentration gradient that would account for the Zeeman splittings of *all* observed excitonic transitions *in all 11 samples* in both σ^+ and σ^- polarizations.

The interface profile satisfying the above conditions is shown schematically in the lower panel of Fig. 5. We model the interface in terms of 4 ML. The 2-ML-thick region D (taken from what is nominally the ZnSe layer of the idealized superlattice) represents the ZnSe region into which Mn ions diffused from the adjacent DMS layer. The 2-ML-thick region I (taken from the $Zn_{1-x}Mn_xSe$ layers of the original

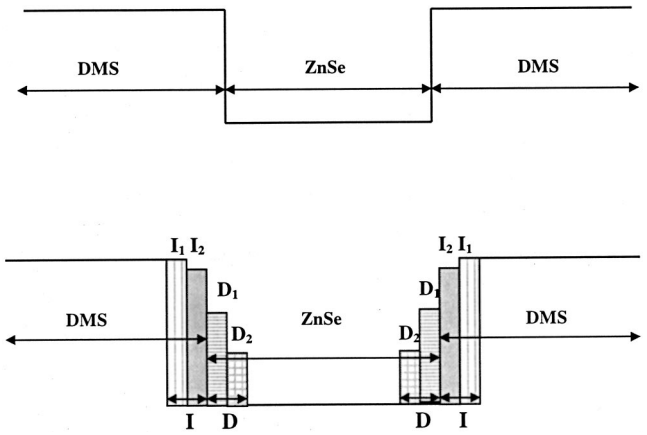

FIG. 5. Modeling of the region near the interface between $Zn_{1-x}Mn_xSe$ and ZnSe, shown schematically in the form of a potential profile for the conduction band. The top diagram shows an abrupt interface. The bottom diagram simulates an interface with graded Mn^{2+} concentration extending over three monolayers. Regions D_1 and D_2 represent two monolayers corresponding to the edge of the original (i.e., abrupt) conduction band well region; and I_1 and I_2 are the first two monolayers of the original barrier.

superlattice) represents the magnetically modified region of the ''original'' $Zn_{1-x}Mn_xSe$ layers. The detailed distribution of x over these four monolayers, forming the graded interface, is modeled as follows. The I_1 layer in Fig. 5 has the same Mn concentration as the DMS barrier material itself (no diffusion). However, we must treat this layer as the interface region because the Mn^{2+} ions in that layer experience an asymmetric neighborhood, with a higher Mn concentration on one side and a lower one on the other. In our fitting procedure we then assume that the Mn concentration in layer I_2 is a fraction y of the value in I_1, due to outdiffusion into region D. Similarly, we take the Mn concentration x in D_1 to be a fraction z_1 of that in I_2, and in layer D_2 we take x to be a fraction z_2 of the concentration in D_1.

In performing the calculations in the presence of magnetic field we used the literature values of α and β for bulk $Zn_{1-x}Mn_xSe$ (see Table II). We also used the same value of T_0 as that obtained by fitting the Zeeman splitting in the measured $Zn_{1-x}Mn_xSe$ ''companion'' epilayer of the corresponding Mn concentration. Thus the only parameter requiring adjustment in the calculations is the value of x_{eff} for each of the sequence of monolayers used to model the diffusion profile near the interface. The calculations were carried out for several different diffusion profiles. To obtain values of x_{eff} that correspond to the concentration x assumed for each layer making up the graded interface we used interface curve in Fig. 3. We then varied the value of x_{eff} of the central DMS layer in order to achieve the best fit to the observed Zeeman splitting of the ground-state exciton. However, certain physical restrictions had to be imposed on the upper and lower limits of that parameter. The upper limit is established by the highest value that x_{eff} can have at an interface (about 0.052 in Fig. 3). The lower limit for a given value of x is established by x_{eff} of the bulk (dashed curve in Fig. 3) since—as shown in that figure—x_{eff} of an interface *always* exceeds the bulk value at any given x.

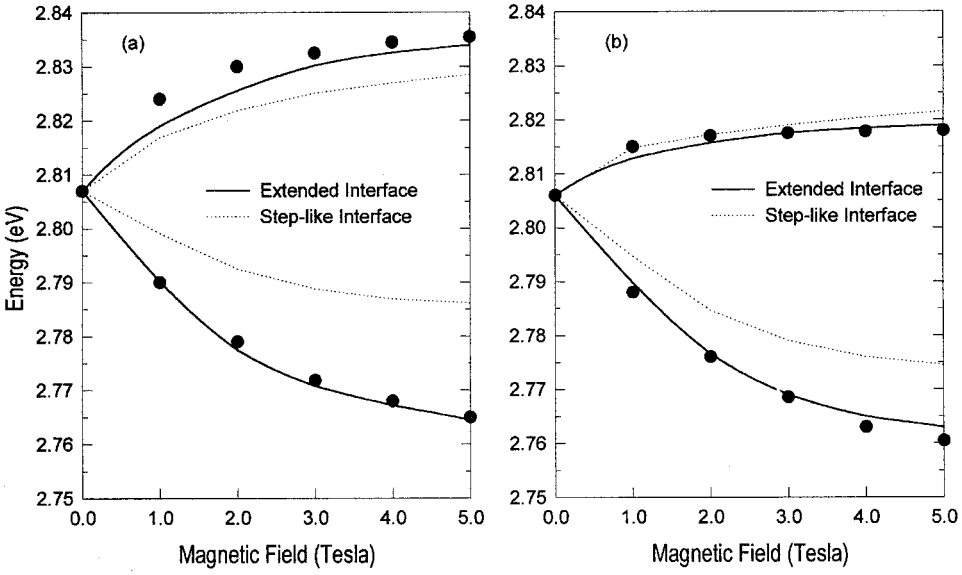

FIG. 6. Transition energies of the Zeeman-split ground state exciton line at $T=1.5$ K for sample 6 [panel (a)] and sample 8 [panel (b)]. Points are experimental; solid curves represent theoretical calculations obtained by assuming an interface profile shown in Fig. 5 (bottom), and using parameters listed in Table III. For comparison we also show the calculated results when a steplike interface is assumed (dotted curves).

We ran the calculations in two iterative steps, keeping in the second iteration the x_{eff} value for the central DMS layer which we found in the first step, and making slight adjustment in the values of x_{eff} for interface regions, with the restriction that these numbers must be the same for all samples within a given series. Our best fits are obtained with the diffusion profiles $y=50\%$, $z_1=60\%$, and $z_2=60\%$. For example, for the series with $x=0.10$ (samples 1–5), the Mn concentration x is still 0.10 in layer I_1, 0.05 in layer I_2, 0.03 in layer D_1, and drops to 0.018 in layer D_2. The thickness of the interface region affected by diffusion extends in our case over 3 ML, which is slightly larger than the 2 ML proposed by Gaj *et al.*[4] for the $CdTe/Cd_{1-x}Mn_xTe$ system, and smaller than the 4 ML proposed by Klar *et al.*[3] for the $ZnTe/Zn_{1-x}Mn_xTe$ and the $ZnSe/Zn_{1-x}Mn_xSe$ systems.

It was pointed out by Gaj *et al.*[4] that diffusion of Mn^{2+} ions occurring during MBE growth may be different for non-DMS layers grown on DMS material (a so-called ''inverted'' interface), and for DMS layers grown on top of a non-DMS material (''normal'' interface), due to the lattice mismatch between the two materials, which would automatically result in an *asymmetric* interface profile. We also tried such asymmetric potential profiles in our calculations. The agreement between experiment and theory was, however, consistently better in the case of symmetrically graded compositions just described.

Since layers I_1 and I_2 are taken from the ''original'' DMS region, and layers D_1 and D_2 from the ZnSe layer (see Fig. 5), the superlattice period itself remains unchanged. The main effect of such grading is that the wells in both DMS and non-DMS layers can no longer be viewed as simple square wells, and approach a parabolic profile. It should be noted that the consequences of such a near-parabolic profile of the wells should be more easily recognized in the case of thin wells than in wider ones, and that such grading should affect the energies of excited states to a much greater degree than that of the ground state.

A. Zeeman splitting of the ground-state transition

In Fig. 6 we compare the Zeeman splittings of the ground-state excitonic transitions observed experimentally for samples 6 and 8 with calculations obtained by assuming a graded interface, as described in Sec IV. One can see that the observed splitting is described quite satisfactorily by the calculations. For comparison we also show the calculated result when steplike interfaces are assumed (dotted line). Table III summarizes the values of x_{eff} used for the interface layers which best describe the experimentally measured Zeeman splittings for all our samples.

It should be noted that the values of x_{eff} for all DMS regions lie between the physically allowed upper and lower limits, as described earlier. Two interesting facts emerge from Table III. First, referring to Fig. 3, we see the general trend that the wider the DMS layer, the closer is its x_{eff} to the bulk (epilayer) value; but as the thickness of the DMS layer is reduced, it behaves increasingly like the interface. This may be expected from the argument that, if the Mn^{2+} ions at

TABLE III. Effective Mn concentration in successive regions near an interface.* Because of the slow variation of x_{eff} with x, we assume a single value of x_{eff} for both I regions, and one for both D regions in Fig. 5.

Sample	$Zn_{1-x}Mn_xSe$ layer thickness (Å)	ZnSe layer thickness (Å)	x_{eff} (region D*)	x_{eff} (region I*)	x_{eff} (DMS)
1	20	60	3.2%	5.1%	5.1%
2	25	25	3.2%	5.1%	4.1%
3	40	80	3.2%	5.1%	5.0%
4	60	40	3.2%	5.1%	4.4%
5	80	40	3.2%	5.1%	4.2%
6	20	40	4.0%	5.1%	5.1%
7	30	30	4.0%	5.1%	4.2%
8	40	80	4.0%	5.1%	5.0%
9	50	50	4.0%	5.1%	4.9%
10	60	40	4.0%	5.1%	4.4%
11	80	40	4.0%	5.1%	4.2%

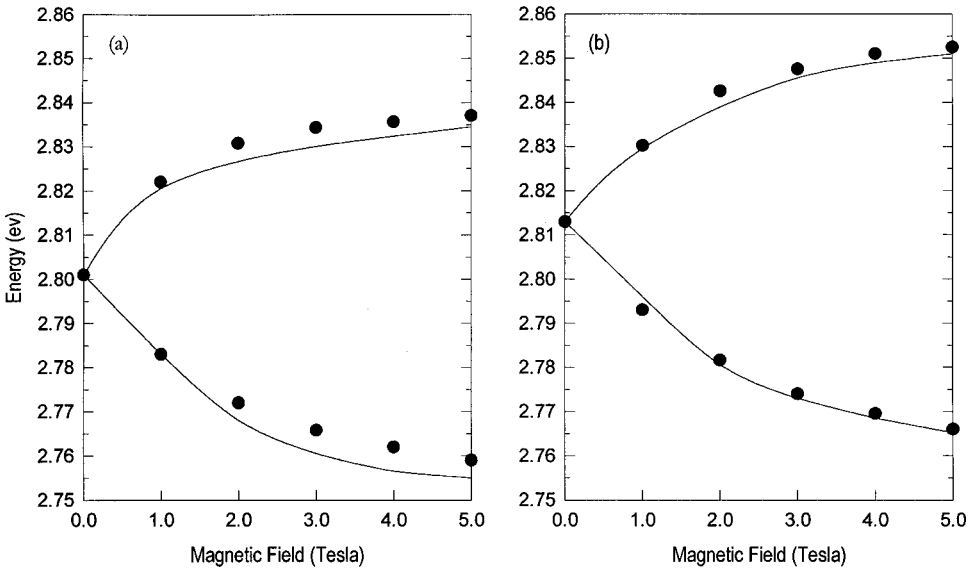

FIG. 7. Transition energies of the Zeeman-split ground state exciton line at $T=1.5$ K for sample 2 [panel (a)] and sample 7 [panel (b)]. Points are experimental; solid curves represent theoretical calculations obtained by assuming an interface profile shown in Fig. 5 (bottom), and magnetic parameters as described in the text.

the interface make a larger contribution to the total average spin per Mn ion than those in the bulk of the DMS layer, clearly the relative number of such ions increases as the DMS layers become thinner, i.e., as its interface-to-volume ratio increases. This is especially obvious in the two superlattices with the thinnest DMS layers (samples 1 and 6), where the values of x_{eff} for the interior of the DMS layer are equal to the values assigned to region *I*.

The second striking fact emerging from Table III, however, is that when the ZnSe layers become very thin, the best-fit values of x_{eff} for the DMS region no longer fit neatly into the scheme where x_{eff} is inversely correlated with the thickness of the DMS layer. This is clearly seen in the case of samples 2 and 7, the superlattices with the shortest periods (50 and 60 Å, respectively). One should note that—since in these structures the nonmagnetic ZnSe layers are very thin—in which the distance between the *D* regions across the ZnSe layer (see Fig. 5) is quite small: 18 Å (circa, 6 ML) for sample 7, and 13 Å (circa 4 ML) for sample 2. At this point one has to take a closer look at the physical assumptions of the model leading to the concept of x_{eff}. The model used here, as mentioned previously, accounts only for the nearest-neighbor antiferromagnetic interactions.[20] However, in samples where the thicknesses of the nonmagnetic layers separating the DMS regions become very small, interactions between the Mn^{2+} ions from neighboring DMS layers may become significant.

While detailed theoretical work needs to be carried out to ascertain the consequences of this effect quantitatively, we have tried to at least qualitatively account for such increase of Mn-Mn antiferromagnetic interactions. We therefore repeated the calculation for samples 2 and 7 as follows. We fixed x_{eff} in the main DMS region to 5.1%, so as to remain consistent with our earlier observations of the inverse correlation between the width of the $Zn_{1-x}Mn_xSe$ layer and its characteristic x_{eff}. Then, in order to reproduce the experimentally observed Zeeman splittings, we had to adjust the progression of x_{eff} for the layers comprising regions *D* and *I*. These are the regions where the Mn ions can become increasingly affected by their magnetic counterparts across the ZnSe layer as that region becomes sufficiently narrow. The final choices of the interface parameters for layers *D* and *I* that best reproduce the observed Zeeman splittings are $x_{\mathrm{eff}}=0.027$ and 0.038, respectively, for sample 2, and $x_{\mathrm{eff}}=0.036$ and 0.046, respectively, for sample 7. Figure 7 shows the fit for these two samples obtained with the above parameters. Note that the modifications in x_{eff} relative to the values listed in Table III are larger for sample 2 than for sample 7. This is consistent with the fact that in sample 2 the *D* layers are closer to each other, so that the antiferromagnetic coupling between the Mn^{2+} ions across the ZnSe layer is expected to be stronger.

In order to achieve good agreement between the calculations and the experimentally observed Zeeman splittings, we also had to adjust the parameter T_o for layers *I* and *D* in samples 2 and 7. As mentioned in Sec. IV, T_o provides a measure of antiferromagnetic interactions between unpaired (''loose'') spins. We achieved the best fit to the data for samples 2 and 7 by using $T_o=2.5$ K, a value higher than that used in the case of all the other superlattices, and also of the epilayers ($T_o=2.15$ K). The fact that samples 2 and 7 require higher values of T_o for layers *I* and *D* is again consistent with the picture of interacting ''loose'' spins across thin ZnSe layer. This result suggests that, when the distance separating the two $Zn_{1-x}Mn_xSe$ layers is reduced to or below 6 ML, we observe the onset of antiferromagnetic interactions across the non-DMS layer. While the existence of Mn-Mn interactions across such distances may be surprising (since these interactions are assumed to be of a short-range nature), we note parenthetically that anomalously long-ranged Mn-Mn interactions have also been reported in the context of neutron scattering in ZnTe/MnTe superlattices,[30] where Mn ions from neighboring MnTe layers have been noted to display spectacular correlations across ZnTe spacers of similar thickness as the ZnSe layers in samples 2 and 7.

B. Zeeman splitting of higher-order transitions

We will now discuss Zeeman splitting of transitions involving excited states, which we also observe in this series of

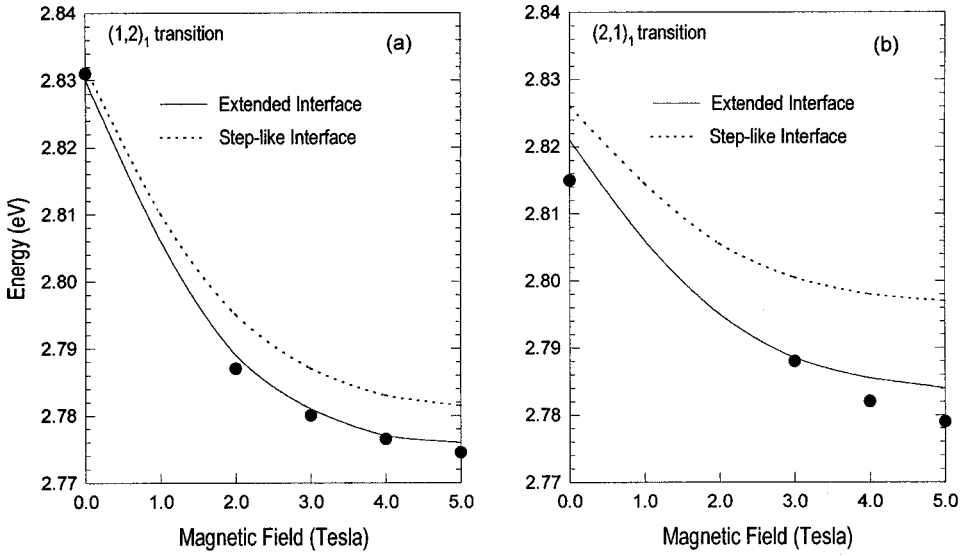

FIG. 8. Magnetic field dependence of transitions from state hh1 to $e2$ at $q=1$ [panel (a)]; and from hh2 to $e1$ at $q=1$ [panel (b)], both observed for sample 5. Points are experimental; solid curves represent theoretical calculations obtained by assuming the graded interface profile shown in Fig. 5 (bottom). For comparison we also show the results calculated when a steplike interface is assumed (dotted curves).

experiments. Figure 1 shows the absorption spectra for sample 5 for the σ^+ circular polarization at different values of magnetic field. Consider the complex absorption line that is made up of three individual, closely lying peaks just to the right of the ground-state exciton line. Of these, the lowest-energy peak (labeled *b*) is identified as the 2*s* ground-state exciton line. In order to identify the two distinct peaks labeled *c* in the figure, we calculated the wave-function overlap between various combinations of initial and final states using the eight-band $\mathbf{k}\cdot\mathbf{p}$ model discussed in Sec. IV. The transitions which have a significant overlap in the energy range of interest are hh1$\rightarrow e2$ at $q=1$ (i.e., at the Brillouin zone edge), designated as $(1,2)_1$; and hh2$\rightarrow e1$ at $q=1$, designated as $(2,1)_1$. One should note here that the superlattices discussed in this paper are *small-offset* superlattices, i.e., they are structures whose excited states are characterized by

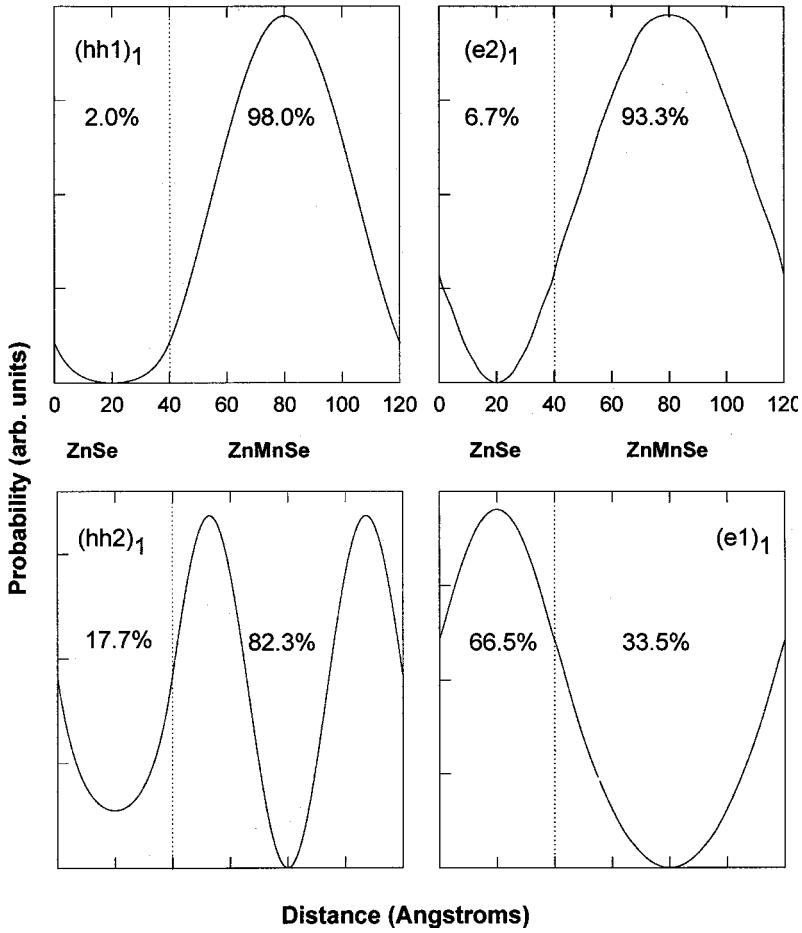

FIG. 9. The probability distribution of the $(\mathrm{hh1})_1$, $(\mathrm{hh2})_1$, $(e2)_1$, and $(e1)_1$ states with spin-down orientation, calculated at 5 Tesla for sample 5. Transitions $(\mathrm{hh1})_1\rightarrow(e2)_1$ and $(\mathrm{hh2})_1\rightarrow(e1)_1$ are observed in the σ^+ polarization. The dotted vertical line corresponds to the nominal boundary between the 40-Å ZnSe layer and the 80-Å ZnMnSe layer. The calculated probability of localization (in percent) is given for each layer.

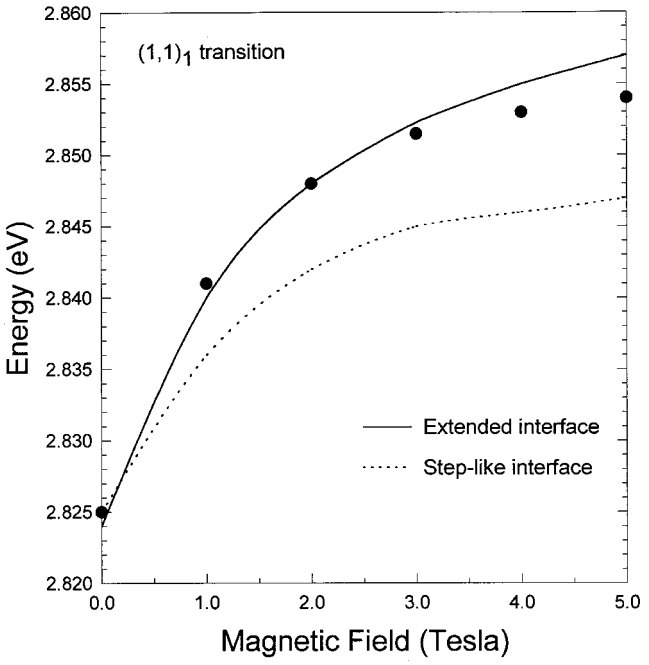

FIG. 10. Magnetic-field dependence of the energy of transition between spin-up hh1 and $e1$ states at $q=1$, observed for sample 11 in the σ^- polarization. Points are experimental, and the solid curve represents the theoretical calculation obtained by assuming a graded interface profile shown in Fig. 5 (bottom). For comparison we also show the results of calculation obtained by assuming a steplike interface (dotted line).

wide subbands separated by narrow minigaps. In this situation transitions which occur at the Brillouin zone center can be readily distinguished from those occurring at the zone edges.[16,31,32]

When calculating the magnetic field dependence of the $(1,2)_1$ and $(2,1)_1$ transition energies, we assumed the extended interface depicted in the lower half of Fig. 5, with all the parameters which best described the Zeeman splitting of the ground-state exciton in a given sample, i.e., without any further adjustment of the parameters. In Figs. 8(a) and 8(b) we show the calculated $(1,2)_1$ and $(2,1)_1$ transition energies (solid curves) and the experimental data (points), respectively, for the case of sample 5. For comparison we also show the calculated result when a steplike interface is assumed (dotted line). It is satisfying to note that the same interface profile which describes the Zeeman splitting of the ground-state exciton also describes the magnetic-field behavior of the higher-order transitions. Of course some discrepancy is expected, because in this case the calculations do not include exciton binding energy corrections.

The difference in the results for the two interface profiles is especially striking in the case of the $(2,1)_1$ transition. This can be understood by looking at Fig. 9, where we plot the probability distribution of the (hh1), (hh2), $(e2)$, and $(e1)$ states at $q=1$ for the spin-down orientation, calculated at 5 T for sample 5. In the case of the $(1,2)_1$ transition the initial (hh1) and the final $(e2)$ states (upper panels) are both mostly localized in the 80 Å-thick $Zn_{1-x}Mn_xSe$ layer, and thus are not particularly sensitive to the shape of the interface profile. However, the situation is quite different for the $(2,1)_1$ transition for that sample. The probability densities of the initial (hh2) and the final $(e1)$ state are in that case quite substantial at the interface (see the lower panel in Fig. 9), so that the magnetic-field dependence of the transition between those two states is expected to be especially sensitive to the details of the interface profile.

The remaining samples examined in this study show similar behavior. Figure 10, for example, shows the energy of the transition between the spin-up hh1 and $e1$ states at the edge of Brillouin zone [designated as $(1,1)_1$] observed in sample 11 in the σ^- circular polarization as a function of applied magnetic field. For this spin orientation the initially type-II band alignment transforms, as the field is increased, into a type-I alignment (see Fig. 4, right-hand diagram), where wells in both the valence and conduction bands correspond to ZnSe layers. Again, the figure shows that the same extended interface describes the Zeeman splitting of this higher-order transition quite well. The fact that at higher fields the calculated transition energies depart slightly from experiment can be explained by the increasing importance of exciton binding energy corrections as the wells grow deeper, a feature that is not included in our calculations.

Again, the point we wish to emphasize is that *the same interface profile* yields energies in quantitative agreement with all observed transitions in all eleven superlattices studied. The magneto absorption results reported here thus provide convincing evidence that in the case of $ZnSe/Zn_{1-x}Mn_xSe$ interfaces the interface profile is graded rather than abrupt, the grading extending over a length of about three monolayers.

VI. CONCLUDING REMARKS

We have studied the Zeeman splitting of the ground-state and higher-order excitonic transitions in a series of 11 $ZnSe/Sn_{1-x}Mn_xSe$ small-offset superlattices. Our quantitative results have shown that the Zeeman splitting observed for all transitions in all eleven superlattices can be successfully explained by a common graded profile of the interface, that extends over a distance of about three monolayers. In the course of this investigation we have also found evidence of antiferromagnetic coupling between Mn ions in different superlattice layers across thin (less than 18 Å) nonmagnetic ZnSe regions.

ACKNOWLEDGMENT

This research was supported by NSF Grant No. DMR00-72897.

[1] W. Grieshaber, A. Haury, J. Gibert, Y. Merle d'Aubigné, A. Wasiela, and J. A. Gaj, Phys. Rev. B **53**, 4891 (1996).
[2] W. Grieshaber, C. Bodin, J. Gibert, J. Gaj, Y. Merle d'Aubigné, A. Wasiela, and G. Feuillet, Appl. Phys. Lett. **63**, 1278 (1994).
[3] P. J. Klar, J. R. Walling, D. Wolverson, J. J. Davies, D. E. Ashenford, and B. Lunn, Semicond. Sci. Technol. **12**, 1240 (1997).
[4] J. A. Gaj, W. Grieshaber, C. Bodin-Deshayes, J. Gibert, G. Feuillet, Y. Merle d'Aubigné, and A. Wasiela, Phys. Rev. B **50**, 5512 (1994).
[5] S. R. Jackson, J. E. Nicholls, W. E. Hagston, P. Harrison, T. Stirner, J. H. C. Hogg, B. Lunn, and D. E. Ashenford, Phys. Rev. B **50**, 5392 (1994).
[6] R. K. Kopf, E. F. Schubert, T. D. Harris, and R. S. Becker, Appl. Phys. Lett. **58**, 631 (1991).
[7] D. Gammon, B. V. Shanabrook, and D. S. Katzer, Phys. Rev. Lett. **67**, 1547 (1991).
[8] B. Jusserand, F. Molot, J.-M. Moison, and G. Le Roux, Appl. Phys. Lett. **57**, 560 (1990).
[9] R. M. Fleming, D. B. McWhan, A. C. Gossard, W. Wiegman, and R. A. Logan, J. Appl. Phys. **51**, 357 (1980).
[10] A. Ourmazd, D. W. Taylor, J. Cunningham, and C. W. Tu, Phys. Rev. Lett. **62**, 933 (1989).
[11] B. Johnson, U. Maier, H. P. Meier, and H. W. M. Salemink, Appl. Phys. Lett. **63**, 1273 (1993).
[12] J. K. Furdyna, J. Appl. Phys. **64**, R29 (1988), and references therein.
[13] L. R. Ram-Mohan, K. H. Yoo, and R. L. Aggarwal, Phys. Rev. B **38**, 6151 (1988).
[14] G. L. Bir and G. E. Pikus, *Symmetry and Strain-Induced Effects in Semiconductors* (Wiley, New York, 1974).
[15] S. Lee, M. Dobrowolska, J. K. Furdyna, H. Luo, and L. R. Ram-Mohan, Phys. Rev. B **54**, 16 939 (1996).
[16] N. Dai, L. R. Ram-Mohan, H. Luo, G. L. Yang, F. C. Zhang, M. Dobrowolska, and J. K. Furdyna, Phys. Rev. B **50**, 18 153 (1994).
[17] L. R. Ram-Mohan, S. Saigal, D. Dossa, and J. Shertzer, Comput. Phys. **4**, 50 (1990).
[18] P. J. Klar, D. Wolverson, J. J. Davis, W. Heimbrodt, and M. Happ, Phys. Rev. B **57**, 7103 (1998).
[19] J. A. Gaj, R. Planel, and G. Fishman, Solid State Commun. **29**, 435 (1979).
[20] J. M. Fatah, T. Piorek, P. Harrison, T. Stirner, and W. E. Hagston, Phys. Rev. B **49**, 10341 (1994).
[21] G. D. Sanders and Y. C. Chang, Phys. Rev. B **32**, 5517 (1985).
[22] Xing-Fei He, Phys. Rev. B **43**, 2063 (1991).
[23] M. Syed, G. L. Yang, J. K. Furdyna, M. Dobrowolska, and J. Kossut, Superlattices Microstruct. **29**, 247 (2001).
[24] S. Lee, F. Michl, U. Rössler, M. Dobrowolska, and J. K. Furdyna, Phys. Rev. B **57**, 9695 (1988).
[25] B. Rockwell, H. R. Chandrasekhar, M. Chandrasekhar, A. K. Ramdas, M. Kobayashi, and R. L. Gunshor, Phys. Rev. B **44**, 11 307 (1991).
[26] X. C. Liu, W. C. Chou, A. Petrou, J. Warnock, B. T. Jonker, G. A. Prinz, and J. J. Krebs, in *Proceedings of the 20th International Conference on the Physics of Semiconductors*, Thessaloniki, edited by E. M. Anastassakis and J. D. Joannopoulos (World Scientific, Singapore, 1990), p. 621.
[27] S. Jackson, W. E. Hagston, P. Harrison, J. H. C. Hagg, J. E. Nicholls, B. Lunn, P. Devine, and S. Ali, Phys. Rev. B **49**, 13 512 (1994).
[28] P. Kossacki, N. T. Khoi, J. A. Gaj, G. Karczewski, T. Wojtowicz, J. Kossut, and K. V. Rao, Solid State Commun. **94**, 439 (1995).
[29] W. J. Ossau and B. Kuhn-Heinrich, Physica B **184**, 422 (1993).
[30] See, e.g., J. Lin, J. J. Rhyne, J. K. Furdyna, and T. M. Giebultowicz, J. Appl. Phys. **83**, 6554 (1998).
[31] G. Yang, L. A. Lewandowski, J. K. Furdyna, and L. R. Ram-Mohan, Acta Phys. Pol. **93**, 567 (1998).
[32] G. Yang, E. Rzepniewski, J. K. Furdyna, and L.-R. Ram-Mohan, Semicond. Sci. Technol. **14**, 878 (1999).